Atmos. Chem. Phys. Discuss., https://doi.org/10.5194/acp-2018-105
Manuscript under review for journal Atmos. Chem. Phys.
Discussion started: 13 February 2018

Atmospheric Chemistry and Physics Discussions

Tropospheric HONO Distribution and Chemistry in the Southeast U.S.

Chunxiang Ye[1,2], Xianliang Zhou[2,3], Dennis Pu[3], Jochen Stutz[4], James Festa[4], Max Spolaor[4], Catalina Tsai[4], Christopher Cantrell[5], Roy L. Mauldin III[5, 6], Andrew Weinheimer[7], Rebecca S. Hornbrook[7], Eric C. Apel[7], Alex Guenther[8], Lisa Kaser[7], Bin Yuan[9, 10], Thomas Karl[11], Julie Haggerty[7], Samuel Hall[7], Kirk Ullmann[7], James Smith[7,12], John Ortega[7]

[1] College of Environmental Sciences and Engineering, Peking University, Beijing, 100871, China

[2] Wadsworth Center, New York State Department of Health, Albany, NY

[3] Department of Environmental Health Sciences, State University of New York, Albany, NY

[4] Department of Atmospheric and Oceanic Sciences, University of California, Los Angeles, CA

[5] Department of Atmospheric and Oceanic Sciences, University of Colorado-Boulder, Boulder Colorado

[6] Department of Physics, University of Helsinki, Helsinki, Finland

[7] National Center for Atmospheric Research, Boulder, Colorado

[8] Department of Earth System Science, University of California, Irvine, CA

[9] NOAA, Earth System Research Laboratory, Chemical Sciences Division, Boulder, Colorado

[10] Cooperative Institute for Research in Environmental Sciences, University of Colorado at Boulder, Boulder, CO, USA

[11] Institute of Atmospheric and Cryospheric Sciences, University of Innsbruck, Innsbruck, Austria

[12] University of Eastern Finland, Kuopio, Finland

Correspondence to: Chunxiang Ye (c.ye@pku.edu.cn) and Xianliang Zhou (xianliang.zhou@health.ny.gov)

Atmos. Chem. Phys. Discuss., https://doi.org/10.5194/acp-2018-105
Manuscript under review for journal Atmos. Chem. Phys.
Discussion started: 13 February 2018

Atmospheric Chemistry and Physics Discussions

Abstract

Here we report the measurement results of nitrous acid (HONO) and a suite of relevant parameters on the NCAR C-130 research aircraft in the Southeast U.S. during NOMADSS 2013 summer field study. Daytime HONO concentrations ranged from low parts per trillion by volume (pptv) in the free troposphere (FT) to mostly within 5 - 15 pptv in the background terrestrial air masses, and to up to 40 pptv in the industrial and urban plumes in the planetary boundary layer (PBL). There was no discernable vertical HONO distribution trend in the PBL above the lowest flight altitude of 300 m, indicating that the ground surface HONO source was not a significant contributor to the HONO budget in the measurement altitude between 300 m and 4.7 km. While there was a strong correlation between the concentrations of HONO and oxides of nitrogen (NO_x = NO + NO_2) (R^2 = 0.52), the sum of all known NO_x-related HONO formation mechanisms was found to account for less 20% of the daytime HONO source in the background terrestrial air masses, due to the low level of NO_x and surface area density of aerosol particles. Photolysis of particulate nitrate (pNO_3) appeared to be the major daytime HONO source in the background terrestrial air masses, based on the measured pNO_3 concentration and the median value of 2.0×10^{-4} s^{-1} for pNO_3 photolysis rate constant determined in the laboratory using ambient aerosol samples collected during the field study. Within the power plant and industrial plumes encountered, daytime HONO was predominantly produced by secondary formation processes involving both NO_x and pNO_3 as precursors. While HONO was not a significant OH precursor compared to O_3 under low NO_x conditions in the air column, it was an important intermediate product of a photochemical renoxification process recycling nitric acid and nitrate back to NO_x. Finally, the HONO/NO_x ratio stayed relatively constant for several hours after sunset in the nocturnal residual layer, suggesting no significant night-time volume HONO source existed in the nocturnal residual layer and the nocturnal FT under background conditions.

1 Introduction

Extensive field studies at ground sites have shown that gas-phase nitrous acid (HONO) exists at much higher levels than expected during the day, with a mixing ratio of HONO up to several parts per billion by volume (ppbv) in the urban atmosphere (Acker et al., 2006; Villena et al., 2011) and up to several hundred parts per trillion by volume (pptv) in rural environments (Acker et al., 2006; Kleffmann et al., 2003; Zhang et al., 2009; Zhou et al., 2002, 2011). At the observed concentrations, HONO photolysis (R1) becomes an important or

Atmos. Chem. Phys. Discuss., https://doi.org/10.5194/acp-2018-105
Manuscript under review for journal Atmos. Chem. Phys.
Discussion started: 13 February 2018

even a major OH primary source in both urban (Elshorbany et al., 2010; Villena et al., 2011) and rural environments near the ground surface (Acker et al., 2006; He et al., 2006; Kleffmann et al., 2003; Zhou et al., 2002, 2011).

$$HONO + h\nu \rightleftharpoons OH + NO \quad \text{(R1, R-1)}.$$

The OH radical is responsible for the removal of primary pollutants, and plays a crucial role in the formation of secondary pollutants, such as O_3 and aerosol (Finlayson-Pitts and Pitts, 2000), and thus HONO, as an important OH precursor, plays an important role in atmospheric chemistry.

The removal processes of HONO from the troposphere are relatively well understood, including mainly photolysis, reaction with the OH radical and surface deposition. Photolysis is the dominant sink for HONO during the day (Kleffmann et al., 2003; Oswald et al., 2015; Zhang et al., 2009, 2012), and dry deposition is the major HONO loss pathway at night, especially over wet surfaces (He et al., 2006;VandenBoer et al., 2015). However, HONO sources in the planetary boundary layer (PBL) are numerous. HONO is directly emitted from combustion processes, such as automobile emissions (Li et al., 2008b) and biomass burning (Burling et al., 2010; Trentmann et al., 2003). Due to the relatively short photolytic lifetime of HONO, in the order of 10 min around summer noontime, the impacts of the direct emission on HONO distribution and chemistry is highly localized and limited to the source region during the day. Recent studies have suggested that microbial activities produce nitrite through nitrification or denitrification in the soil, and soil emission may be a significant HONO source for the overlying atmosphere (Maljanen et al., 2013; Oswald et al., 2013; Su et al., 2011). Since the emission of HONO from soils depends on multiple factors, such as the abundance of soil nitrate and ammonia, the soil pH and water content, and microbial types and activities, it is expected that the strength of this HONO emission varies greatly in different environments and thus needs to be further quantified (Oswald et al., 2013).

HONO is a unique species that is produced through heterogeneous reactions of different precursors, such as NO_2 and HNO_3, on surfaces (R2 - R3):

$$NO_2 + H_2O \text{ (or organics)} \xrightarrow{\text{surface}} HONO \quad \text{(R2)}$$

$$HNO_3(s) + h\nu \xrightarrow{\text{organics},H_2O} HONO + NO_2 \quad \text{(R3)}$$

Heterogeneous reactions of NO_2 with organics (R2) on the surfaces have been found to be greatly accelerated by sunlight through photosensitization (George et al., 2005; Kleffmann, 2007; Stemmler et al., 2006, 2007) and these reactions are likely the major daytime HONO

source in urban environments (Acker et al., 2006; Villena et al., 2011; Wong et al., 2011). Laboratory studies have confirmed that HNO_3 undergoes photolysis in sunlight at rates 2 - 3 orders of magnitude greater on the surface than in the gas phase (Baergen and Donaldson, 2013; Du and Zhu, 2011; Ye et al., 2016a, b; Zhou et al., 2003; Zhu et al., 2008), producing NO_x and HONO. In low-NO_x environments, photolysis of nitric acid/nitrate deposited on the surface has been proposed to be the major daytime HONO source near the ground surface (Ye et al., 2016b; Zhou et al., 2003, 2011).

Several processes within an air mass may lead to volume, or *in situ*, production of HONO. The OH+NO reaction (R-1) in the gas phase may be a significant HONO source in high NO_x and photochemically reactive atmospheres (Kleffmann, 2007; Villena et al., 2011), but becomes negligible in low-NO_x environments(Li et al., 2014; Ye et al., 2016b). Two additional gas-phase reactions have been also proposed to produce HONO within the air column: between excited NO_2 (NO_2^*) and water vapor (R4) (Li et al., 2008a), and between NO_2 and the hydroperoxyl-water complex ($HO_2 \cdot H_2O$) (R5a) (Li et al., 2014):

$$NO_2^* + H_2O \rightarrow HONO + OH \quad \text{(R4)}$$

$$HO_2 \cdot H_2O + NO_2 \xrightarrow{\alpha} HONO + O_2 + H_2O \quad \text{(R5a)}$$

$$HO_2 \cdot H_2O + NO_2 \xrightarrow{1-\alpha} \text{products} \quad \text{(R5b)}$$

However, further laboratory evidence suggests that reaction (R4) is too slow to be important (Carr et al., 2009; Wong et al., 2011). And recent airborne observations have demonstrated that the HONO yield (α) from reaction (R5) is less than 0.03 (Ye et al., 2015).

Almost all HONO measurements to date have been made at ground stations. The observed HONO concentrations reported in the literature represent the HONO levels in the lower PBL under the significant but varying influence of ground surface processes. Thus, it is difficult to distinguish the ground surface HONO sources from the *in situ* HONO sources. Measurements of the vertical profile of HONO concentrations and/or HONO fluxes have suggested that ground surfaces can be major HONO sources for the overlying atmosphere in many cases (He et al., 2006; Kleffmann et al., 2003 Stutz et al., 2002; Zhou et al., 2011), but not in some other cases (Villena et al., 2011). A recent HONO flux measurement has suggested that the HONO source from the forest canopy contributed ~ 60% of the measured HONO budget at the measurement height of 11 m above the forest canopy, and the *in situ* HONO production contributed the remaining ~ 40% (Zhou et al., 2011). Similarly, observational and modeling studies implied a presence of a volume HONO source at 130-m

altitude above Houston, TX (Wong et al., 2012, 2013). The relative importance of *in situ* HONO production would be expected to increase with altitude due to decreasing influence of the ground surface, at least during the day. Airborne measurements in the air mass above the altitude influenced directly by ground HONO sources should provide more direct and quantitative evidence for *in situ* HONO production in the troposphere. Indeed, the limited number of airborne measurements available have shown that HONO exists in substantial amounts throughout the troposphere (Li et al., 2014; Ye et al., 2015; Zhang et al., 2009).

Here we report airborne HONO measurement results and findings from five research flights in the Southeast U.S. during the NOMADSS (Nitrogen, Oxidants, Mercury and Aerosol Distributions, Sources and Sinks) 2013 summer field campaign aboard the NSF/NCAR C-130 research aircraft.

2 Experimental

NOMADSS was an airborne field study under the "umbrella" of SAS (Southeast Atmosphere Study). It consisted of nineteen research flights on board the NSF/NCAR C-130 aircraft from June 1, 2013 to July 15, 2013. Parameters observed included HONO, HNO_3, particulate nitrate, NO_x, O_3, BrO, OH radicals, HO_2 radicals, RO_2 radicals, aerosol surface area densities (size <1 μm), VOCs, photolysis frequencies, and other meteorology parameters. Table 1 summarizes the instrumentation, time resolution, detection limit, accuracy, and references for the measurements.

HONO was measured by two long-path absorption photometric (LPAP) systems based on the Griess-Saltzman reaction (Zhang et al., 2012; Ye et al., 2016b). Briefly, ambient air was first brought into the aircraft through an inlet and then HONO was scrubbed using de-ionized (DI) water in a 10-turn glass coil sampler to ensure high efficiency HONO sampling. The scrubbed nitrite was then derivatized with 5 mM sulfanilamide (SA) and 0.5 mM N-(1-Naphthyl)-ethylene-diamine (NED) in 40 mM HCl, to form an azo dye within 5 min. The azo dye was detected by light absorbance at 540 nm using an optic fiber spectrometer (LEDSpec, WPI) with a 1-m liquid waveguide capillary flow cell (WPI). "Zero-HONO" air was generated by directing the sample stream through a Na_2CO_3-coated denuder to remove HONO and was sampled by the systems periodically to establish measurement baselines. Interference from NO_x, PAN, and particulate nitrite if any, was corrected by subtracting the baseline from the ambient air signal. Due to the low collecting efficiency of these interfering species in the sampling coil and their low concentrations, the combined interference was estimated to be less

than 10% of the total signal. Potential interference from peroxynitric acid (HO_2NO_2) was suppressed by heating the PFA sampling line to 50 °C with a residence time of 0.8 s. The HO_2NO_2 steady state concentration was estimated to be less than 1 pptv at temperatures of 20 - 30 °C in the background PBL (Gierczak et al., 2005), and thus interference from HO_2NO_2 was negligible. Whereas in power plant plumes and urban plumes in the PBL or biomass burning plumes in the upper free troposphere (FT), HO_2NO_2 interference was not negligible. HONO measurements were corrected by a term of "$0.2 \times [HO_2NO_2]_{SS}$", assuming an upper limit HO_2NO_2-to-HONO conversion efficiency of 0.2 in our system. $[HO_2NO_2]_{SS}$ refers to the steady state concentration of HO_2NO_2, and the upper limit HO_2NO_2-to-HONO conversion efficiency of 0.2 was estimated from the ratio of the observed [HONO] to the calculated $[HO_2NO_2]_{SS}$ in cold, high altitude air masses under our measurement conditions. In the PBL, the correction is below 10% of the total signal. The accuracy of HONO measurements was confirmed by comparison with a limb-scanning Differential Optical Absorption Spectroscopy (DOAS) (Platt and Stutz, 2008). The agreement between these two instruments was very good in wide power plant plumes where HONO mixing ratios significantly exceeded the detection limits of both instruments (Ye et al., 2016b).

Particulate nitrate (pNO_3) was quantitatively collected with a frit disc sampler after a NaCl-coated denuder to remove HNO_3 (Huang et al., 2002). The collected nitrate was reduced to nitrite by a Cd column, and determined using a LPAP systems (Zhang et al., 2012). Zero air was generated to establish measurement baselines for pNO_3 by passing the ambient air through a Teflon filter and a NaCl-coated denuder to remove aerosol particles and HNO_3. Potential interferences from HONO, NO_x and PAN were corrected by subtracting the baselines from the ambient air signals.

The mixing ratios of a large number of non-methane organic compounds (NMOCs) were measured by Trace Organic Gas Analyzer (TOGA) (Hornbrook et al., 2011a) and Proton-transfer-reaction mass spectrometry (PTR-MS) (Karl et al., 2003; de Gouw and Warneke, 2007). The surface area density of fine particles was measured by a Scanning Mobility Particle Sizer (SMPS). The photolysis frequencies were determined by a Charged-coupled device Actinic Flux Spectroradiometer instrument (CAFS) (Shetter et al., 2002). The mixing ratios of HO_x and RO_2 radicals were measured by a method based on selected-ion chemical-ionization mass spectrometry (SICIMS) (Hornbrook et al., 2011b; Mauldin et al., 2010). The mixing ratios of ozone and NO_x were measured by NCAR's chemiluminescence

instruments (Ridley et al., 2004). Meteorology parameters were provided by state parameter measurements on board the C-130.

The results from five out of nineteen flights are presented here to discuss vertical HONO distribution and HONO chemistry in the Southeast U.S. The flight tracks are shown in Figure 1.

3 Results and Discussion

3.1 General data description

Figure 2 shows the time series of HONO, NO_x, pNO_3 concentrations and the measurement altitude for five selected research flights in the Southeast U.S. during the NOMADSS 2013 summer field study. Research flight (RF) #4, RF #5 and RF #17 are race track flights in the background terrestrial areas designed to establish HONO distribution and explore HONO chemistry in background air masses. RF #11 is a race track flight designed to intercept plumes from local power plants and urban areas and explore HONO chemistry therein. All four flights were conducted in the daytime, roughly from 14:00 to 22:00 UTC (10:00 to 18:00 EDT). RF #18 is a race track flight conducted from 20:30 on July 12th to 03:30 on July 13th UTC (16:30 on July 12th to 00:30 on July 13th, 2013 EDT), aiming to study the potential night-time HONO accumulation both in the PBL and the FT.

Table 2 summarizes the data statistics for HONO, NO_x and pNO_3 measurements in the PBL and the FT, and Figure 3 shows composite vertical distributions of HONO, NO_x and pNO_3 concentrations from the five flights in the Southeast U.S. during the NOMADSS 2013 summer field study. HONO, NO_x and pNO_3 concentrations show horizontal gradients in every race track flight and vary in different race track flights, reflecting the inhomogeneity of air masses in the region. However, no significant vertical gradient in HONO, NO_x and pNO_3 concentrations is apparent, which will be further discussed below. Except in a few power plant plumes and urban plumes mostly encountered in RF #11 (labelled as A-G), most of the data is representative of background terrestrial air masses. The range of the mixing ratio of HONO is 1.1 – 35.9 pptv. The mean (±1SD) and median values of HONO concentration are 5.4 (±3.4) pptv and 4.2 pptv in the FT, and 11.2 (±4.3) pptv and 10.6 pptv in the PBL. HONO levels at ~ 4 pptv are typically found in the background FT, but high HONO concentrations up to 18.2 pptv are also observed in the elevated biomass burning plumes. Many biomass burning plumes were observed during other flights and will be discussed in a future paper. HONO levels at ~ 11 pptv are representative of background conditions in the

PBL. High HONO levels up to 35.9 pptv are observed in the power plant plumes and urban plumes in RF #11. The HONO distribution and chemistry in these urban and power plant plumes in the Southeast U.S. are specifically discussed below, in comparison with the results for background conditions (RF # 4, #5, and #17). These measured HONO values are consistent with the range of 4 – 74 pptv in the troposphere over Northern Michigan (Zhang et al., 2009), but are significantly lower than other airborne observations (up to 150 pptv) in the morning residual layer over an industrial region of Northern Italy (Li et al., 2014), where the levels of HONO precursors, such as NO_x and pNO_3, were much higher.

The range of the mixing ratio of NO_x is from several pptv to around 1.6 ppbv. The mean (±1SD) and median values of NO_x concentration are 96 (±52) pptv and 92 pptv in the FT, and 313 (±174) pptv and 278 pptv in the PBL. The mixing ratios of NO_x are mostly between 50 - 150 pptv in the background conditions in the FT and between 200 - 500 pptv in the background conditions in the PBL. Similar to HONO, high values of NO_x also occur in the urban and power plant plumes in the PBL (up to 1.6 ppbv) and in the biomass burning plumes in the FT (up to 0.6 ppbv).

Fewer measurement data points are available for pNO_3, compared to those for NO_x and HONO, due to air bubble formation in the flow cell of the pNO_3 system, especially at high altitudes. The range of the mixing ratio of pNO_3 is from 2 pptv to 216 pptv, with the mean (±1SD) and median values of 28 (±25) pptv and 21 pptv in the FT, and 78 (±47) pptv and 70 pptv in the PBL. The pNO_3 levels were highly variable in both the FT and the PBL. In the FT, the pNO_3 levels were often under 10 pptv, but high concentrations up to 115 pptv were also observed in elevated biomass burning plumes. In the PBL, high pNO_3 levels were sometimes observed in relative clean conditions; whereas, low pNO_3 levels were observed in high HONO and NO_x power plant plumes. Both the N(V) level (= $[HNO_3]$ + $[pNO_3]$) and the partitioning between HNO_3 and pNO_3 seem to play roles in determining the pNO_3 level.

3.2 HONO contribution from ground-level sources

There are several ground-level HONO sources that may contribute to the HONO budget in the overlying atmosphere. They include anthropogenic sources, such as power plant and automobile emissions (Li et al., 2008b), and natural processes, such as soil emission (Maljanen et al., 2013; Oswald et al., 2013; Su et al., 2011), heterogeneous reactions of NO_2 (Acker et al., 2006; George et al., 2005; Ndour et al., 2008, 2009; Ramazan et al., 2006) and

surface HNO_3 photolysis (Ye et al., 2016b; Zhou et al., 2003,2011). Since HONO photolytic lifetime is relatively short, e.g. 8 - 16 min in RF #4, RF #5, RF #11 and RF #17, a steep negative vertical gradient of HONO concentration would be expected if a significant contribution originated from the ground. The lack of a significant vertical gradient in the measured HONO concentrations (Fig. 3) thus suggests that the ground contribution is either limited to the shallow layer of the boundary layer near the ground, below the C-130 lowest flight altitude of 300 m, or small relative to the *in situ* production of HONO in the air column (Ye et al., 2017).

To further examine the potential HONO contribution from the ground sources, vertical profiles of HONO, NO_x, and pNO_3, are compared with those of potential temperature (K) and isoprene measured, for example, in the first race-track of RF#4 from 11:00 – 12:15 LT (Fig. 4). Indeed, the measurements conducted in the PBL from 300 m to 1200 m were above the unstable surface layer, as indicated by the constant potential temperature (Fig. 4e). The vertical distribution of isoprene originating from the ground can be expressed with the following equation (Eq.1):

$$\ln\left(\frac{C}{C_0}\right) = -\frac{k\tau}{H}h = -\frac{h}{h^*} \qquad \text{(Eq. 1)}$$

where, C_o and C are its concentrations near the ground and at the altitude h, k is the pseudo-first order degradation rate constant, H is the boundary layer height, τ is the average mixing time in the PBL, and h^* (= $H/(k\tau)$) is its characteristic transport height within one degradation lifetime of isoprene. According to the best fit of (Eq.1) to the observed isoprene data (Fig. 4d), its characteristic transport height h^* is estimated 692 m for isoprene. Assuming isoprene is mainly oxidized by the OH radical whose average concentration is estimated at 3×10^6 mole cm^{-3} in the PBL (Kaser et al., 2015), the pseudo-first order degradation rate constant of ~ 3.0×10^{-4} s^{-1} (or the degradation rate of ~ 0.93 h^{-1}) is determined for isoprene. Based on a boundary layer height of ~1.2 km (Fig. 4e), an average PBL mixing time τ is estimated to be ~1.6 h between 11:00 – 12:15 LT of RF #4. With a photolytic lifetime of ~ 11 min for HONO, the estimated characteristic transport height of HONO is 138 m between 11:00 – 12:15 LT in RF #4, well below 300 m, the lowest flight altitude of the C-130 aircraft during this field study. Therefore, the instrument on-board the C-130 would not detect the HONO contribution from the ground sources during this race-track profiling around noontime. However, it is interesting to note that there was a slight increase in HONO concentration at the two lowest altitudes (Fig. 4a), which may be attributed to the increasing concentrations of its precursors, NO_x and pNO_3 (Fig. 4b, c), both which are much longer lived than HONO.

Apart from the rapid photolytic loss of HONO, the rate of vertical mixing plays an important role in limiting the transport height of HONO in the PBL. The vertical mixing of the PBL is enhanced from the morning to the afternoon, as the ground surface is heated by solar radiation gradually during the day. The average mixing time in the PBL is reduced from ~ 3 h in the morning, to ~ 1.5 h around noontime, and to ~ 30 min in the afternoon, determined from isoprene gradients from RF #4, #5 and #17. The characteristic transport height of HONO would be ~ 500 m in the afternoon, i.e., some of the ground emitted HONO could survive and be transported to lower measurement altitudes, and thus may be detected by our profile measurements. However, the contribution from ground HONO sources to the observed HONO concentrations in the PBL above 300 m appear to be limited, as indicated by the lack of consistent vertical HONO gradient above the altitude of 300 m (Fig. 3a) in all the race track flights

3.3 Daytime HONO chemistry in low NO_x areas

After removing the data measured in the urban and power plant plumes, the daytime HONO concentrations are mostly within the range of 5 - 15 pptv throughout the PBL in the background terrestrial areas in the five race-track research flights. Photolysis of HONO is its dominant sink, with a photolysis lifetime of 8 - 16 min during these four daytime flights (RF #4, RF #5, RF #11, and RF #17). Therefore, there must be a significant volume HONO source, up to 200 pptv h^{-1}, within the air mass to sustain the observed HONO concentrations.

Both NO_x and pNO_3 are potential HONO precursors in the air column. Figure 5 shows the correlation analysis of HONO with NO_x and pNO_3 in the background terrestrial air masses during the five flights. While HONO correlates relatively well with NO_x ($r^2 = 0.52$), with a fitted HONO/NO_x ratio around 0.04, it only weakly correlates with pNO_3 ($R^2 = 0.14$) (Fig. 5). It may appear at first that NO_x is a more important HONO precursor than pNO_3. However, the detailed analysis below suggests that NO_x is only a minor precursor to the observed HONO, and photolysis of pNO_3 is the major *in situ* HONO source.

The photo-stationary state HONO concentration ($[HONO]_{pss}$) was calculated using Equation 2 that takes into account all the known HONO source contributions from NO_x-related reactions, including gaseous reactions of OH and NO (R-1), excited NO_2 (NO_2*) and water vapor (R4) (Carr et al., 2009; Li et al., 2008a), NO_2 and the hydroperoxyl-water complex ($HO_2 \cdot H_2O$) with an upper limit HONO yield of 3% (R5a)(Li et al., 2014; Ye et al., 2015), and heterogeneous reaction of NO_2 on aerosol surfaces (R2) using an upper limit

uptake coefficient of 10^{-4} reported in the literature (George et al., 2005; Monge et al., 2010; Ndour et al., 2008, 2009; Stemmler et al., 2006, 2007):

$$[HONO]_{pss} = \frac{k_{-1}[NO][OH]+k_4[NO_2^*][H_2O]+\alpha k_5[NO_2^*][H_2O]+k_2 S_{aerosol}[NO_2]}{J_{HONO}+k_{OH-HONO}[OH]} \quad \text{(Eq. 2)}$$

where $S_{aerosol}$ is the aerosol surface area density. Under typical daytime conditions in the PBL with the median measured values of reactants, the upper limit $[HONO]_{pss}$ value is less than 2 pptv, much lower than the median measured HONO concentration of ~ 11 pptv. Figure 6a shows the relationship (r^2 = 0.44) between the photolytic HONO loss rate with the sum of HONO production rates from all the NO_x-related reactions calculated with upper-limit reaction rate constants. A slope of about 0.19 indicates that the contribution from these NO_x-related reactions to the volume HONO source is minor in the background troposphere, despite the good correlation between HONO and NO_x. The high HONO/NO_x ratios up to 0.24 in the low-NO_x air masses are indicative of more important contributions from other HONO precursors, such as pNO_3.

Photolysis of HNO_3 on surfaces has been found to proceed at a much higher rate than in the gas phase (Baergen and Donaldson, 2013; Du and Zhu, 2011; Ramazan et al., 2004; Ye et al., 2016b; Zhou et al., 2003; Zhu et al., 2008), with HONO as the major product on environmental surfaces (Ye et al., 2016a, 2017). Furthermore, photolysis of particulate nitrate has been found to be the major daytime HONO source in the marine boundary layer (Ye et al., 2016b). To examine the role of particulate nitrate as a potential HONO source in the troposphere, aerosol samples over the terrestrial areas were collected on Teflon filters on board the C-130 aircraft during the NOMADSS 2013 summer field study and were used in the light-exposure experiments to determine the photolysis rate constants for particulate nitrate in the laboratory. The determined pNO_3 photolysis rate constant ($J^N_{pNO_3}$) varies over a wide range, from 8.3×10^{-5} s^{-1} to 3.1×10^{-4} s^{-1}, with a median of 2.0×10^{-4} s^{-1} and a mean (± 1 standard deviation) of 1.9 (± 1.2) × 10^{-4} s^{-1}, when normalized to tropical noontime conditions at ground level (solar zenith angle = 0 °), and the average HONO to NO_2 relative yield is 2.0 (Ye et al., 2017). Figure 6b shows the relationship between the photolytic HONO loss rate ($J_{HONO} \times [HONO]$) and the volume HONO production rates from pNO_3 photolysis ($2/3 \times J_{pNO3} \times [pNO_3]$). The median $J^N_{pNO_3}$ of ~ 2.0×10^{-4} s^{-1} was used to calculate the ambient J_{pNO_3} by scaling to J_{HNO3}:

$$J_{pNO_3} = J^N_{pNO3} \times \frac{J_{HNO_3}}{7.0\times10^{-7}\ s^{-1}} \quad \text{(Eq. 3),}$$

where J_{HNO_3} is the photolysis rate constant of gas-phase HNO_3 calculated from light intensity measurement on the C-130 aircraft, and 7.0×10^{-7} s^{-1} is the photolysis rate constant of gas-phase HNO_3 under the tropical noontime condition at ground level (solar zenith angle = 0 °). A slope of 0.67 can be derived from Figure 6b, suggesting that pNO_3 photolysis is the major volume HONO source. However, the r^2 of 0.31 is not as strong as expected from pNO_3 photolysis being the major volume HONO source. The lower than expected correlation coefficient may be due to the fact that only a single median J^N_{pNO3} value of ~ 2.0×10^{-4} s^{-1} is used in the calculations of the ambient J_{pNO_3} and the production rates of HONO in Figure 6b, while the actual pNO_3 photolysis rate constants determined from seven NOMADSS aerosol samples are highly variable, ranging from 8.3×10^{-5} s^{-1} to 3.1×10^{-4} s^{-1} (Ye et al., 2017). The production rates of HONO in Figure 6b are thus only rough estimates of the *in situ* HONO production rates from pNO_3 photolysis in different air masses.

HONO photolysis has been found to be an important or even a major OH primary source in the atmosphere near the ground surface (Elshorbany et al., 2010; He et al., 2006; Kleffmann et al., 2003; Villena et al., 2011; Zhou et al., 2011). However, HONO is not a significant daytime OH precursor in the background troposphere away from the ground surface. Based on the measurement results in this study, the contribution of HONO photolysis to the OH source budget (mean ± SD) is 52 ± 22 pptv h^{-1} in the PBL and 28 ± 20 pptv h^{-1} in the FT, respectively, less than 10% of the OH production contributed by O_3 photolysis. However, since HONO is mainly produced from photolysis of particulate nitrate, it becomes an important intermediate product of a photochemical renoxification process recycling nitric acid and nitrate back to NO_x. The regenerating rate of NO_x of about 52 pptv h^{-1} via HONO photolysis is equivalent to an air column NO_x source of ~ 2×10^{-6} mol m^{-2} h^{-1} in the 1- km PBL, a considerable supplementary NO_x source in the low-NO_x background area.

3.4 HONO chemistry in plumes

One of the objectives of RF #11 was to study the chemistry of HONO in urban and coal fired power plant plumes. The arrows and corresponding labels in Figures 2 and 7 indicate the urban plumes (A – C) and power plant plumes (D - G). Benzene was used as the tracer of urban plumes (Liu et al., 2012; Shaw et al., 2015). Benzene peaks were observed in all urban plumes (A – C), but not in the power plant plumes (D – G). The power plant plumes were generated from high-intensity point sources, and thus had features of narrow but high peaks of both HONO and NO_x concentrations in the time-series plots (Figs. 2 and 7). In contrast, the

urban plumes were generated from area sources and thus were shown as broad peaks of HONO and NO_x in the time-series plot with low levels of NO_x (mostly below 500 pptv) (Fig. 2). There were a few sharp but small NO_x peaks within the broad urban plumes, reflecting the contributions of some point sources in the urban areas. The observed HONO/NO_x ratio was around 0.02 in the power plant plumes, lower than that of ~ 0.05 in urban plumes and in background terrestrial air masses. Based on the distances between measurement locations from the power plants or the centre of urban area and the observed wind speed, the transport times of these power plant plumes were estimated to be ≥1 h, over 5 times longer than HONO photolysis lifetime of 8 - 16 min. Therefore, most of the observed HONO in the power plant plumes was produced *in situ* within the air masses. Since the typical emission ratio of HONO/NO_x is less than 0.01 in the fresh power plant plumes and automobile engines (Kurtenbach et al., 2001; Li et al., 2008b), the elevated HONO/NO_x ratios observed in the plumes suggest the presence of other HONO precursors, such as pNO_3.

Figure 7b shows the time-series plot of HONO budget within the air masses sampled by the C-130 aircraft during flight RF# 11, comparing its photolysis loss rate with its production rates from pNO_3 photolysis and from all the NO_x-related reactions combined. Photolysis of particulate nitrate appears to be the major volume HONO source in all urban plumes and in most of the power plant plumes except for plume G observed here (Fig. 7b). NO_x was generally more important as a HONO precursor in the power plant plumes than in the urban plumes and in low-NO_x background terrestrial air masses, due to higher levels of NO_x (up to 1.6 ppb in Fig. 7a), OH radical and aerosol surface density. For example, all the NO_x-related reactions combined contributed up to 52% of the total volume HONO source required to sustain the observed HONO concentration in plume G (Fig. 7b). In fresh power plant plumes encountered during the RF #7 to Ohio River Valley (X. Zhou, unpublished data), over 20 ppb NO_x was detected, and the NO_x-related reactions were found to account for almost all the required HONO source to sustain the observed HONO. The power plant plumes undergo rapid physical and photochemical evolution during the day, such as dilution and NO_x-into-HNO_3 conversion. Thus, the relative contributions from NO_x-related reactions and particulate nitrate photolysis as HONO sources change rapidly as the plumes age.

3.5 Night-time HONO chemistry

HONO accumulation near the ground surface during the nighttime has been widely observed (Kleffmann et al., 2003; Oswald et al., 2015; 2008; Stutz et al., 2002, 2010; VandenBoer et

al., 2013, 2014, 2015), contributed by various anthropogenic and natural HONO sources on the ground. The main objective of RF #18 was to study the night-time HONO evolution in both the nocturnal residual layer and the nocturnal FT. After sunset, the surface cooling promotes the formations of a inversion layer near the ground surface and a nocturnal residual layer above; the contribution from ground HONO sources then becomes negligible to the air masses beyond the surface inversion layer. Meanwhile, no effective HONO sinks, such as photolysis, oxidation by OH and dry deposition, exist in the nocturnal residual layer. Thus the HONO accumulation, if any, is a net contribution from dark heterogeneous NO_2 reaction on aerosol surfaces (R2).

The C-130 flew in an elongated race track pattern along a north-south direction, about 140 km from Nashville, TN (Fig. 1), alternating between the PBL (1200 m) and the FT (2500 m), from late afternoon to midnight local time (Fig. 2). In the FT, HONO and NO_x concentrations were relatively stable throughout the afternoon and the night, staying around 4 ppt and 90 pptv respectively. The lack of night-time HONO accumulation is expected from the low levels of HONO precursors, mostly NO_2, and surface area of aerosol particles in the FT (Fig. 2).

The conditions in the PBL were far more variable and complicated. There were strong horizontal gradients of NO_x, pNO_3 and HONO in the PBL, with higher concentrations at the southern end and lower concentrations at the northern end of the flight track. Back-trajectory analysis using NOAA's HYSPLIT model (Stein et al., 2015) indicates that the encountered air masses in the PBL at the southern end passed over Nashville, about 140 km northeast of the sample area, with a transport time of about 6 h (Fig. 8a), while the air masses at the northern end stayed to north of Nashville (Fig. 8b). Therefore, the anthropogenic emissions from the metropolitan area of Nashville contributed to the higher concentrations of pollutants observed at the southern end of the flight track. There were also trends of increasing concentrations of NO_x, pNO_3 and HONO with time after the sunset (Fig. 2). This was probably a result of less dispersion and dilution of anthropogenic pollutants, including NO_x, as the PBL became more stable after sunset. Furthermore, as time progressed from late afternoon into evening and night, the air masses were less photochemically aged during the transport from the source areas, due to the decreasing solar light intensity and shorter solar light exposure time.

Because of the large spatial and temporal variations in the concentrations of HONO and its precursors in the PLB (Fig. 2), it is difficult to directly evaluate the nighttime HONO accumulation from HONO measurements alone. The concentration ratio of HONO and its

dominant nighttime precursor, NO_2, can be used as an indicator of nighttime HONO accumulation. As the air masses at measurement altitude of 1200 m decoupled from the ground-level processes after sunset, the HONO production from heterogeneous NO_2 reaction (R2) on aerosol surface becomes the only HONO source, and can be expressed by the following equations (Eq. 4 and Eq. 5):

$$P(HONO) = \frac{1}{4} \times \left[\frac{S}{V}\right] \times \sqrt{\frac{8RT}{\pi M}} \times \gamma \times [NO_2] \quad \text{(Eq.4)}$$

$$\frac{P(HONO)}{[NO_2]} = \frac{1}{4} \times \left[\frac{S}{V}\right] \times \sqrt{\frac{8RT}{\pi M}} \times \gamma \quad \text{(Eq.5)}$$

where $\left[\frac{S}{V}\right]$ is the specific aerosol surface area density, R is the gas constant, K the absolute temperature, M the molecular weight of NO_2, and γ is the dark uptake coefficient of NO_2 leading to HONO production. The NO_2-normalized HONO accumulation over time, $\Delta\frac{[HONO]}{[NO_2]}$, can then be calculated by equation (Eq. 6):

$$\Delta\frac{[HONO]}{[NO_2]} \sim \frac{1}{4} \times \left[\frac{S}{V}\right] \times \sqrt{\frac{8RT}{\pi M}} \times \gamma \times \Delta t \quad \text{(Eq. 6)}$$

Assuming a dark uptake coefficient γ of 1×10^{-5} of NO_2 on aerosol (George et al., 2005; Monge et al., 2010; Ndour et al., 2008; Stemmler et al., 2006, 2007) with a $\left[\frac{S}{V}\right]$ value of ~10^{-4} m^{-1}, a relative HONO accumulation rate, $\Delta\frac{[HONO]}{[NO_2]}/\Delta t$ of ~0.0003 h^{-1} is estimated using the equation (Eq. 6), equivalent to a HONO accumulation of 0.13 pptv hr^{-1} at a constant NO_2 concentration of 400 pptv. Such a low HONO accumulation rate is below our measurement detection limit. Indeed, the calculated HONO to the NO_x ratio using the measurement data stayed almost unchanged with time (Fig. 9), well within the observational variability after the sunset, suggesting no significant volume production of HONO in the nocturnal boundary layer.

4 Conclusions

Substantial levels of HONO existed during the day in both the PBL (median ~ 11 pptv) and the FT (median ~ 4 pptv) over the Southeast U.S. during the NOMADSS 2013 summer field study. It appears that ground HONO sources did not significantly contribute to the HONO budget in the PBL above the minimum measurement heights of 300 m. Photolysis of particulate nitrate was the major volume HONO source in the background low-NO_x air masses, while NO_x was only a minor HONO precursor. Up to several tens pptv of HONO

were observed in coal fired power plant plumes and urban plumes during the day; the major HONO precursor could be either NO_x or pNO_3 depending on the chemical characteristics and photochemical age of the plumes. No significant night-time HONO accumulation was observed in the nocturnal residual layer and the free troposphere, suggesting no significant night-time volume HONO source due to low levels of NO_x and specific aerosol surface area. HONO was not a significant daytime OH precursor in the rural troposphere away from the ground surface; however, HONO mainly produced from photolysis of particulate nitrate could significant provide a renoxification pathway. The NO_x regeneration rate of about 52 pptv h^{-1} in rural PBL is a considerable supplementary NO_x source in a low-NO_x background region.

Acknowledgements

This research is funded by National Science Foundation (NSF) grants (AGS-1216166, AGS-1215712, and AGS-1216743). We would like to acknowledge operational, technical, and scientific support provided by NCAR, sponsored by the National Science Foundation. The data are available in our project data archive (http://data.eol.ucar.edu/master_list/?project=SAS). Any opinions, findings, and conclusions or recommendations expressed in this paper are those of the authors and do not necessarily reflect the views of NSF.

References

Acker, K., Moller, D., Wieprecht, W., Meixner, F. X., Bohn, B., Gilge, S., Plass-Dulmer, C., and Berresheim, H.: Strong daytime production of OH from HNO_2 at a rural mountain site, Geophys. Res. Lett., 33, Artn L02809,10.1029/2005gl024643, 2006.

Baergen, A. M., and Donaldson, D. J.: Photochemical renoxification of nitric scid on real urban grime, Environ. Sci. Technol., 47, 815-820, 10.1021/es3037862, 2013.

Burling, I. R., Yokelson, R. J., Griffith, D. W. T., Johnson, T. J., Veres, P., Roberts, J. M., Warneke, C., Urbanski, S. P., Reardon, J., Weise, D. R., Hao, W. M., and de Gouw, J.: Laboratory measurements of trace gas emissions from biomass burning of fuel types from the southeastern and southwestern United States, Atmos. Chem. Phys., 10, 11115-11130, 2010.

Carr, S., Heard, D. E., and Blitz, M. A.: Comment on "Atmospheric hydroxyl radical production from electronically excited NO_2 and H_2O", Science, 324, 2009.

de Gouw, J., and Warneke, C.: Measurements of volatile organic compounds in the earths atmosphere using proton-transfer-reaction mass spectrometry, Mass Spectrom. Rev., 26, 223-257, 2007.

Du, J., and Zhu, L.: Quantification of the absorption cross sections of surface-adsorbed nitric acid in the 335-365 nm region by Brewster angle cavity ring-down spectroscopy, Chem. Phys. Lett., 511, 213-218, 10.1016/j.cplett.2011.06.062, 2011.

Elshorbany, Y. F., Kleffmann, J., Kurtenbach, R., Lissi, E., Rubio, M., Villena, G., Gramsch, E., Rickard, A. R., Pilling, M. J., and Wiesen, P.: Seasonal dependence of the oxidation capacity of the city of Santiago de Chile, Atmos. Environ., 44, 5383-5394, 10.1016/j.atmosenv.2009.08.036, 2010.

Finlayson-Pitts, B. J., and J. N. Pitts, Jr.: Chemistry of the Upper and Lower Atmosphere: Theory, Experiments, and Applications, Academic Press, San Diego, California, 2000.

Flagan, R. C.: Electrical mobility methods for sub-micrometer particle characterization. In Aerosol Measurement: Principles, Techniques, and Applications, Third Edition (eds P. Kulkarni, P. A. Baron and K. Willeke), pp339-364, John Wiley & Sons, New York, 2002.

George, C., Strekowski, R. S., Kleffmann, J., Stemmler, K., and Ammann, M.: Photoenhanced uptake of gaseous NO_2 on solid-organic compounds: a photochemical source of HONO?, Faraday Discuss., 130, 195-210, 2005.

495 Gierczak, T., Jimenez, E., Riffault, V., Burkholder, J. B., and Ravishankara, A. R.: Thermal
496 decomposition of HO_2NO_2 (peroxynitric acid, PNA): Rate coefficient and determination of
497 the enthalpy of formation, J. Phys. Chem. A, 109, 586-596, 2005.
498 Handley, S. R., Clifford, D., and Donaldson, D. J.: Photochemical loss of nitric acid on
499 organic films: A possible recycling mechanism for NO_x, Environ. Sci. Technol., 41, 3898-
500 3903, 10.1021/es062044z, 2007.
501 He, Y., Zhou, X. L., Hou, J., Gao, H. L., and Bertman, S. B.: Importance of dew in controlling
502 the air-surface exchange of HONO in rural forested environments, Geophys. Res. Lett., 33,
503 2006.
504 Hornbrook, R. S., Blake, D. R., Diskin, G. S., Fried, A., Fuelberg, H. E., Meinardi, S.,
505 Mikoviny, T., Richter, D., Sachse, G. W., Vay, S. A., Walega, J., Weibring, P.,
506 Weinheimer, A. J., Wiedinmyer, C., Wisthaler, A., Hills, A., Riemer, D. D., and Apel, E.
507 C.: Observations of nonmethane organic compounds during ARCTAS - Part 1: Biomass
508 burning emissions and plume enhancements, Atmos. Chem. Phys., 11, 11103-11130,
509 2011a.
510 Hornbrook, R. S., Crawford, J. H., Edwards, G. D., Goyea, O., Mauldin, R. L., Olson, J. S.,
511 and Cantrell, C. A.: Measurements of tropospheric HO_2 and RO_2 by oxygen dilution
512 modulation and chemical ionization mass spectrometry, Atmos. Meas. Tech., 4, 735-756,
513 2011b.
514 Huang, G., Zhou, X., Deng, G., Qiao, H., and Civerolo, K.: Measurements of atmospheric
515 nitrous acid and nitric acid, Atmos. Environ., *36*, 2225-2235, 2002.
516 Kaser, L., Karl, T., Yuan, B., Mauldin, R. L. III, Cantrell, C. A., Guenther, A. B., Patton, E.
517 G., Weinheimer, A. J., Knote, C., Orlando, J., Emmons, L., Apel, E., Hornbrook, Shertz,
518 R., S., Ullmann, K., Hall, S., Graus, M., de Gouw, J., Zhou, X., and Ye, C.: chemistry-
519 turbulence interactions and mesoscale variability influence the cleansing efficiency of the
520 atmosphere, Geophys. Res. Lett., 42, doi:10.1002/2015GL066641, 2015.
521 Karl, T., Jobson, T., Kuster, W.C., Williams, E., Stutz, J., Shetter, R., Hall, S.R., Goldan, P.,
522 Fehsenfeld, F., and W. Lindinger, W.: The use of Proton-Transfer-Reaction Mass
523 Spectrometry to Characterize VOC Sources at the La Porte Super Site during the Texas Air
524 Quality Study 2000, J. Geophys. Res., 108, doi: 10.1029/2002JD003333, 2003.
525 Kleffmann, J., Kurtenbach, R., Lorzer, J., Wiesen, P., Kalthoff, N., Vogel, B., and Vogel, H.:
526 Measured and simulated vertical profiles of nitrous acid - Part I: Field measurements,
527 Atmos. Environ., 37, 2949-2955, 2003.

528 Kleffmann, J.: Daytime sources of nitrous acid (HONO) in the atmospheric boundary layer,
529 Chemphyschem, 8, 1137-1144, 10.1002/cphc.200700016, 2007.
530 Kurtenbach, R., Becker, K. H., Gomes, J. A. G., Kleffmann, J., Lorzer, J. C., Spittler, M.,
531 Wiesen, P., Ackermann, R., Geyer, A., and Platt, U.: Investigations of emissions and
532 heterogeneous formation of HONO in a road traffic tunnel, Atmos. Environ., 35, 3385-
533 3394, Doi 10.1016/S1352-2310(01)00138-8, 2001.
534 Li, S. P., Matthews, J., and Sinha, A.: Atmospheric hydroxyl radical production from
535 electronically excited NO_2 and H_2O, Science, 319, 1657-1660, 2008a.
536 Li, X., Rohrer, F., Hofzumahaus, A., Brauers, T., Haseler, R., Bohn, B., Broch, S., Fuchs, H.,
537 Gomm, S., Holland, F., Jager, J., Kaiser, J., Keutsch, F. N., Lohse, I., Lu, K. D., Tillmann,
538 R., Wegener, R., Wolfe, G. M., Mentel, T. F., Kiendler-Scharr, A., and Wahner, A.:
539 Missing gas-phase source of HONO inferred from Zeppelin measurements in the
540 troposphere, Science, 344, 292-296, 2014.
541 Li, Y. Q., Schwab, J. J., and Demerjian, K. L.: Fast time response measurements of gaseous
542 nitrous acid using a tunable diode laser absorption spectrometer: HONO emission source
543 from vehicle exhausts, Geophys. Res. Lett., 35, 2008b.
544 Liu, W., Hsieh, H., Chen, S., Chang, J.S., Lin, N., Chang, C., and Wang, J.: Diagnosis of air
545 quality through observation and modeling of volatile organic compounds (VOCs) as
546 pollution tracers. Atmos. Environ., 55, 56-63, 2012.
547 Maljanen, M., Yli-Pirila, P., Hytonen, J., Joutsensaari, J., and Martikainen, P. J.: Acidic
548 northern soils as sources of atmospheric nitrous acid (HONO), Soil. Biol. Biochem., 67,
549 94-97, 10.1016/j.soilbio.2013.08.013, 2013.
550 Mauldin, R., Kosciuch, E., Eisele, F., Huey, G., Tanner, D., Sjostedt, S., Blake, D., Chen, G.,
551 Crawford, J., and Davis, D.: South Pole Antarctica observations and modeling results: New
552 insights on HOx radical and sulfur chemistry, Atmos. Environ., 44, 572-581, 2010.
553 Monge, M. E., D'Anna, B., Mazri, L., Giroir-Fendler, A., Ammann, M., Donaldson, D. J., and
554 George, C.: Light changes the atmospheric reactivity of soot, P. Natl. Acad. Sci. USA, 107,
555 6605-6609, 2010.
556 Ndour, M., D'Anna, B., George, C., Ka, O., Balkanski, Y., Kleffmann, J., Stemmler, K., and
557 Ammann, M.: Photoenhanced uptake of NO_2 on mineral dust: Laboratory experiments and
558 model simulations, Geophys. Res. Lett., 35, 2008.

559 Ndour, M., Nicolas, M., D'Anna, B., Ka, O., and George, C.: Photoreactivity of NO_2 on
560 mineral dusts originating from different locations of the Sahara desert, Phys. Chem. Chem.
561 Phys., 11, 1312-1319, 2009.
562 Oswald, R., Behrendt, T., Ermel, M., Wu, D., Su, H., Cheng, Y., Breuninger, C., Moravek,
563 A., Mougin, E., Delon, C., Loubet, B., Pommerening-Roser, A., Sorgel, M., Poschl, U.,
564 Hoffmann, T., Andreae, M. O., Meixner, F. X., and Trebs, I.: HONO emissions from soil
565 bacteria as a major source of atmospheric reactive nitrogen, Science, 341, 1233-1235,
566 10.1126/science.1242266, 2013.
567 Oswald, R., Ermel, M., Hens, K., Novelli, A., Ouwersloot, H. G., Paasonen, P., Petaja, T.,
568 Sipila, M., Keronen, P., Back, J., Konigstedt, R., Beygi, Z. H., Fischer, H., Bohn, B.,
569 Kubistin, D., Harder, H., Martinez, M., Williams, J., Hoffmann, T., Trebs, I., and Sorgel,
570 M.: A comparison of HONO budgets for two measurement heights at a field station within
571 the boreal forest in Finland, Atmos. Chem. Phys., 15, 799-813, 10.5194/acp-15-799-2015,
572 2015.
573 Platt, U., and Stutz, J: Differential Optical Absorption Spectroscopy: Principles and
574 Applications, Springer, Berlin,, 2008.
575 Ramazan, K. A., Syomin, D., and Finlayson-Pitts, B. J.: The photochemical production of
576 HONO during the heterogeneous hydrolysis of NO_2, Phys. Chem. Chem. Phys., 6, 3836-
577 3843, 10.1039/b402195a, 2004.
578 Ramazan, K. A., Wingen, L. M., Miller, Y., Chaban, G. M., Gerber, R. B., Xantheas, S. S.,
579 and Finlayson-Pitts, B. J.: New experimental and theoretical approach to the heterogeneous
580 hydrolysis of NO2: Key role of molecular nitric acid and its complexes, J. Phys. Chem. A,
581 110, 6886-6897, 10.1021/jp056426n, 2006.
582 Ridley, B., Ott, L., Pickering, K., Emmons, L., Montzka, D., Weinheimer, A., Knapp, D.,
583 Grahek, F., Li, L., Heymsfield, G., McGill, M., Kucera, P., Mahoney, M. J., Baumgardner,
584 D., Schultz, M., and Brasseur, G.: Florida thunderstorms: A faucet of reactive nitrogen to
585 the upper troposphere, J. Geophys. Res.-Atmos., 109, 2004.
586 Shaw, M. D., Lee, J. D., Davison, B., Vaughan, A., Purvis, R. M., Harvey, A.; Lewis, A. C.,
587 and Hewitt, C. N.: Airborne determination of the temporo-spatial distribution of benzene,
588 toluene, nitrogen oxides and ozone in the boundary layer across Greater London, UK.
589 Atmos. Chem. Phys., 15, 5083–5097, 2015.

590 Shetter, R. E., Cinquini, L., Lefer, B. L., Hall, S. R., and Madronich, S.: Comparison of
591 airborne measured and calculated spectral actinic flux and derived photolysis frequencies
592 during the PEM Tropics B mission, J. Geophys. Res.-Atmos., 108, 2002.
593 Stemmler, K., Ammann, M., Donders, C., Kleffmann, J., and George, C.: Photosensitized
594 reduction of nitrogen dioxide on humic acid as a source of nitrous acid, Nature, 440, 195-
595 198, 10.1038/nature04603, 2006.
596 Stemmler, K., Ndour, M., Elshorbany, Y., Kleffmann, J., D'Anna, B., George, C., Bohn, B.,
597 and Ammann, M.: Light induced conversion of nitrogen dioxide into nitrous acid on
598 submicron humic acid aerosol, Atmos. Chem. Phys., 7, 4237-4248, 2007.
599 Stein, A. F., Draxler, R. R., Rolph, G. D., Stunder, B. J. B., Cohen, M. D., and Ngan, F.:
600 NOAA's HYSPLIT atmospheric transport and dispersion modeling system. Bul. Amer.
601 Meteorol. Soc., 96, 2059-2077, 10.1175/BAMS-D-14-00110.1, 2015.
602 Stutz, J., Alicke, B., and Neftel, A.: Nitrous acid formation in the urban atmosphere: Gradient
603 measurements of NO_2 and HONO over grass in Milan, Italy, J. Geophys. Res.-Atmos.,
604 107, Artn 8192,10.1029/2001jd000390, 2002.
605 Stutz, J., Oh, H. J., Whitlow, S. I., Anderson, C., Dibbb, J. E., Flynn, J. H., Rappengluck, B.,
606 and Lefer, B.: Simultaneous DOAS and mist-chamber IC measurements of HONO in
607 Houston, TX, Atmos. Environ., 44, 4090-4098, 2010.
608 Su, H., Cheng, Y. F., Oswald, R., Behrendt, T., Trebs, I., Meixner, F. X., Andreae, M. O.,
609 Cheng, P., Zhang, Y., and Poschl, U.: Soil Nitrite as a Source of Atmospheric HONO and
610 OH Radicals, Science, 333, 1616-1618, 10.1126/science.1207687, 2011.
611 Trentmann, J., Andreae, M. O., and Graf, H. F.: Chemical processes in a young biomass-
612 burning plume, J. Geophys. Res.-Atmos., 108, 2003.
613 VandenBoer, T. C., Brown, S. S., Murphy, J. G., Keene, W. C., Young, C. J., Pszenny, A. A.
614 P., Kim, S., Warneke, C., de Gouw, J. A., Maben, J. R., Wagner, N. L., Riedel, T. P.,
615 Thornton, J. A., Wolfe, D. E., Dube, W. P., Ozturk, F., Brock, C. A., Grossberg, N., Lefer,
616 B., Lerner, B., Middlebrook, A. M., and Roberts, J. M.: Understanding the role of the
617 ground surface in HONO vertical structure: High resolution vertical profiles during
618 NACHTT-11, J. Geophys. Res.-Atmos., 118, 10155-10171, 2013.
619 VandenBoer, T. C., Markovic, M. Z., Sanders, J. E., Ren, X., Pusede, S. E., Browne, E. C.,
620 Cohen, R. C., Zhang, L., Thomas, J., Brune, W. H., and Murphy, J. G.: Evidence for a
621 nitrous acid (HONO) reservoir at the ground surface in Bakersfield, CA, during CalNex
622 2010, J. Geophys. Res.-Atmos., 119, 9093-9106, 10.1002/2013JD020971, 2014.

VandenBoer, T. C., Young, C. J., Talukdar, R. K., Markovic, M. Z., Brown, S. S., Roberts, J. M., and Murphy, J. G.: Nocturnal loss and daytime source of nitrous acid through reactive uptake and displacement, Nature Geosci., 8, 55-60, 2015.

Villena, G., Kleffmann, J., Kurtenbach, R., Wiesen, P., Lissi, E., Rubio, M. A., Croxatto, G., and Rappengluck, B.: Vertical gradients of HONO, NO_x and O_3 in Santiago de Chile, Atmos. Environ., 45, 3867-3873, 2011.

Wong, K. W., Oh, H. J., Lefer, B. L., Rappengluck, B., and Stutz, J.: Vertical profiles of nitrous acid in the nocturnal urban atmosphere of Houston, TX, Atmos. Chem. Phys., 11, 3595-3609, 2011.

Wong, K. W., Tsai, C., Lefer, B., Haman, C., Grossberg, N., Brune, W. H., Ren, X., Luke, W., and Stutz, J.: Daytime HONO vertical gradients during SHARP 2009 in Houston, TX, Atmos. Chem. Phys., 12, 635-652, 2012.

Wong, K. W., Tsai, C., Lefer, B., Grossberg, N., and Stutz, J.: Modeling of daytime HONO vertical gradients during SHARP 2009, Atmos. Chem. Phys., 13, 3587-3601, 2013.

Ye, C. X., Zhou, X. L., Pu, D., Stutz, J., Festa, J., Spolaor, M., Cantrell, C., Mauldin, R. L., Weinheimer, A., and Haggerty, J.: Comment on "Missing gas-phase source of HONO inferred from Zeppelin measurements in the troposphere", Science, 348, 10.1126/science.aaa1992, 2015.

Ye, C. X., Gao, H. L., Zhang, N., and Zhou, X.: Photolysis of nitric Acid and nitrate on natural and artificial surfaces, Environ. Sci. Technol., 50, 3530-3536, 2016a.

Ye, C. X., Zhou, X. L., Pu, D., Stutz, J., Festa, J., Spolaor, M., Tsai, C., Cantrell, C., Mauldin, R. L., Campos, T., Weinheimer, A., Hornbrook, R. S., Apel, E. C., Guenther, A., Kaser, L., Yuan, B., Karl, T., Haggerty, J., Hall, S., Ullmann, K., Smith, J. N., Ortega, J., and Knote, C.: Rapid cycling of reactive nitrogen in the marine boundary layer, Nature, 532, 489-491, 2016b.

Ye, C., Zhang, N., Gao, H., and Zhou, X.: Photolysis of particulate nitrate as a source of HONO and NO_x, Environ Sci Technol, DOI: 10.1021/acs.est.7b00387, 2017.

Zhang, N., Zhou, X., Shepson, P. B., Gao, H., Alaghmand, M., and Stirm, B.: Aircraft measurement of HONO vertical profiles over a forested region, Geophys. Res. Lett., 36, Artn L15820,10.1029/2009gl038999, 2009.

Zhang, N., Zhou, X., Bertman, S., Tang, D., Alaghmand, M., Shepson, P. B., and Carroll, M. A.: Measurements of ambient HONO concentrations and vertical HONO flux above a northern Michigan forest canopy, Atmos. Chem. Phys., 12, 8285-8296, 2012.

656 Zhou, X., Civerolo, K., Dai, H., Huang, G., Schwab, J., and Demerjian, K.: Summertime
657 nitrous acid chemistry in the atmospheric boundary layer at a rural site in New York State,
658 *J. Geophys. Res.*, *107*, doi:10.1029/2001JD001539, 2002.
659 Zhou, X., Gao, H., He, Y., Huang, G., Bertman, S. B., Civerolo, K., and Schwab, J.: Nitric
660 acid photolysis on surfaces in low-NOx environments: Significant atmospheric
661 implications, Geophys. Res. Lett., 30, Artn 2217,10.1029/2003gl018620, 2003.
662 Zhou, X., Zhang, N., TerAvest, M., Tang, D., Hou, J., Bertman, S., Alaghmand, M., Shepson,
663 P. B., Carroll, M. A., Griffith, S., Dusanter, S., and Stevens, P. S.: Nitric acid photolysis on
664 forest canopy surface as a source for tropospheric nitrous acid, Nature Geosci., 4, 440-443,
665 10.1038/NGEO1164, 2011.
666 Zhu, C. Z., Xiang, B., Zhu, L., and Cole, R.: Determination of absorption cross sections of
667 surface-adsorbed HNO(3) in the 290-330 nm region by Brewster angle cavity ring-down
668 spectroscopy, Chem. Phys. Lett., 458, 373-377, 2008.
669
670

Atmos. Chem. Phys. Discuss., https://doi.org/10.5194/acp-2018-105
Manuscript under review for journal Atmos. Chem. Phys.
Discussion started: 13 February 2018

Atmospheric Chemistry and Physics Discussions

671 Table 1. Measurements from the NOMADSS 2013 summer study used in this analysis.

Parameters	Instrument	Time Resolution	Detection Limit	Accuracy	References
HONO	LPAP	200 s	1 pptv	20%	(1, 2)
pNO_3	LPAP	360 s	2 pptv	30%	(1, 2, 3)
HNO_3	LPAP	20 min	2 pptv	30%	(1, 2, 3)
NO	CI	1 s	20 pptv	10%	(4)
NO_2	CI	1 s	40 pptv	15%	(4)
O_3	CI	1 s	100 pptv	5%	(4)
OH	SICIMS	30 s	$*5\times10^4$	30%	(5, 6)
HONO	DOAS	60 s	~ 30 pptv	20%	(7)
Photolysis Frequencies	CAFS	6 s		10-15%	(8)
Surface area density	SMPS/UHSAS	65 s/1 s		20%	(9)
VOCs	PTRMS	15 s		20%	(10, 11)
VOCs/organic nitrates	TOGA	20 s		20%	(12)

672 ***in molecules cm^{-3}
673 LPAP: long-path absorption photometric (LPAP) systems
674 CI: 4-channel chemiluminescence instrument
675 SICIMS: selected-ion chemical-ionization mass spectrometer
676 DOAS: Differential Optical Absorption Spectroscopy
677 CAFS: Charged-coupled device Actinic Flux Spectroradiometer
678 SMPS: Scanning Mobility Particle Sizer
679 UHSAS: Ultra-High Sensitivity Aerosol Spectrometer
680 PTRMS: Proton Transfer Reaction Mass Spectrometry
681 TOGA: Trace Organic Gas Analyzer
682 References: (1) Zhang et al., 2012; (2) Ye et al., 2016b; (3) Huang et al., 2002; (4) Ridley et
683 al., 2004; (5) Hornbrook et al., 2011b; (6) Mauldin et al., 2010; (7) Platt and Stutz, 2008;
684 (8) Shetter et al., 2002; (9) Flagan, 2011; (10) Karl et al., 2003; (11) de Gouw and
685 Warneke, 2007; (12) Hornbrook et al., 2011a.

Atmos. Chem. Phys. Discuss., https://doi.org/10.5194/acp-2018-105
Manuscript under review for journal Atmos. Chem. Phys.
Discussion started: 13 February 2018

Atmospheric Chemistry and Physics Discussions

686 Table 2. Data statistics for HONO, NO_x and pNO_3 measurements both in the PBL and the FT
687 from the five Southeast U.S. research flights during the NOMADSS 2013 summer field study.

		HONO, pptv	NO_x, pptv	pNO_3, pptv
PBL	Range	3.1 - 35.9	81 - 1635	7 - 216
	Mean ± SD	11.2 ± 4.3	313 ± 174	79 ± 47
	Median	10.6	278	70
FT	Range	1.1 - 18.2	<10 - 582	2 - 115
	Mean(±SD)	5.4 ± 3.4	96 ± 52	28 ± 25
	Median	4.2	92	21

688

Atmos. Chem. Phys. Discuss., https://doi.org/10.5194/acp-2018-105
Manuscript under review for journal Atmos. Chem. Phys.
Discussion started: 13 February 2018

Atmospheric Chemistry and Physics Discussions

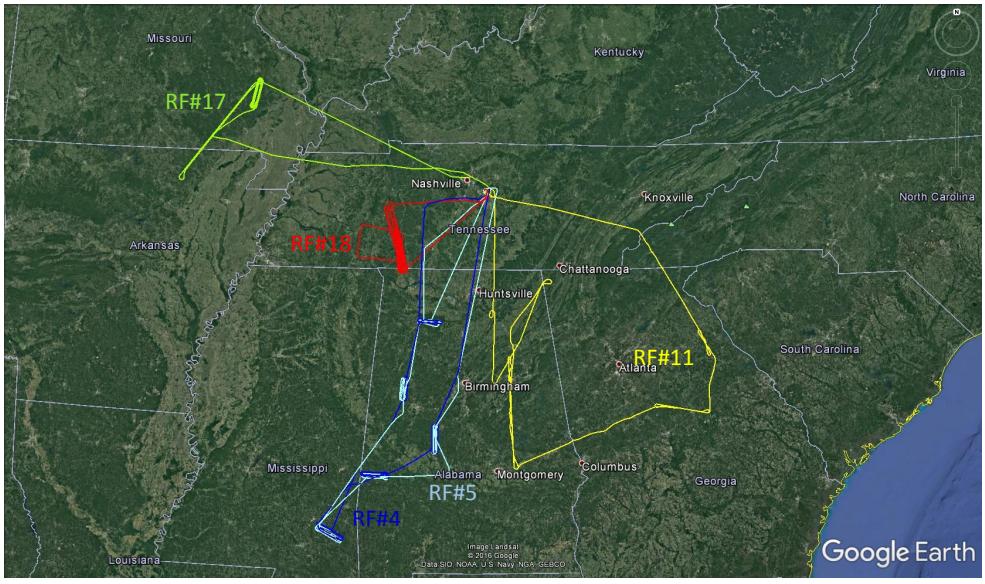

Figure 1. Flight tracks in the Southeast US during the NOMADSS 2013 summer study. The flight start time and end time in UTC (= EDT+4)) are: RF#4 (blue): 15:12 and 22:30, June 12, 2013; RF#5 (light blue): 15:04 and 21:52, June 14, 2013; RF#11 (yellow): 15:20 and 21:02, June 29, 2013; RF#17 (green): 15:07 and 21:57, July 11, 2013; RF#18 (red): 20:32, July 12, 2013, and 03:37, July 13, 2013

Atmos. Chem. Phys. Discuss., https://doi.org/10.5194/acp-2018-105
Manuscript under review for journal Atmos. Chem. Phys.
Discussion started: 13 February 2018

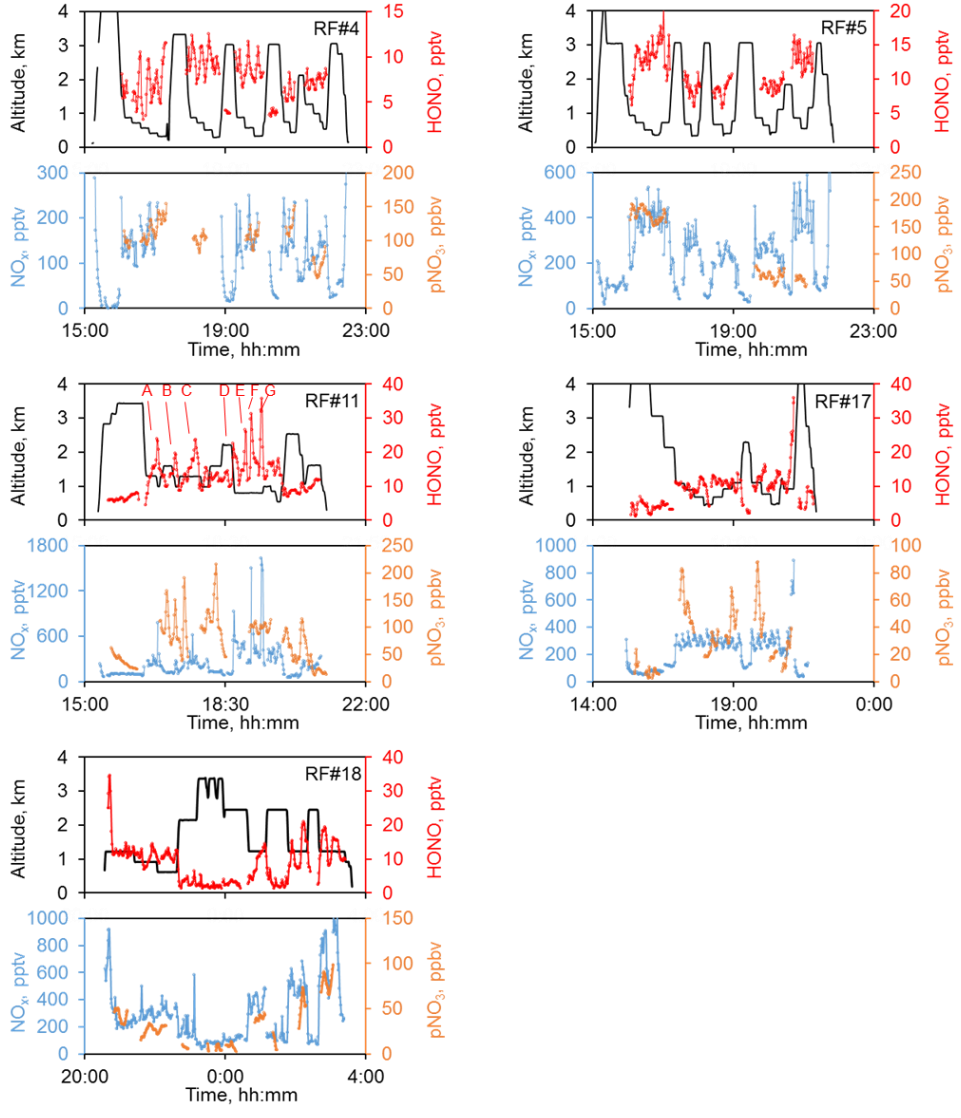

Figure 2. Time series of altitude, HONO, NO_x and pNO_3 in five flights (RF #4, RF #5, RF #11, RF #17 and #18) in the Southeast US during the NOMADSS 2013 summer study. In RF #11, A-C indicate urban plumes, and D-G indicate coal-fired power plant plumes. The time is in UTC.

Atmos. Chem. Phys. Discuss., https://doi.org/10.5194/acp-2018-105
Manuscript under review for journal Atmos. Chem. Phys.
Discussion started: 13 February 2018

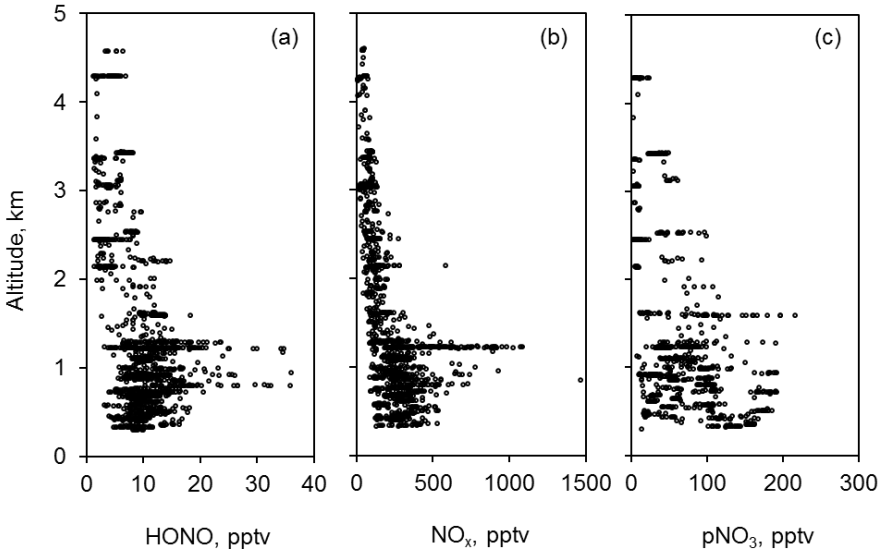

Figure 3. Vertical distributions of concentrations of HONO (a), NO_x (b), and pNO_3 (c) in the five selected flights in the Southeast US during the NOMADSS 2013 summer study.

Atmos. Chem. Phys. Discuss., https://doi.org/10.5194/acp-2018-105
Manuscript under review for journal Atmos. Chem. Phys.
Discussion started: 13 February 2018

Atmospheric Chemistry and Physics Discussions

707

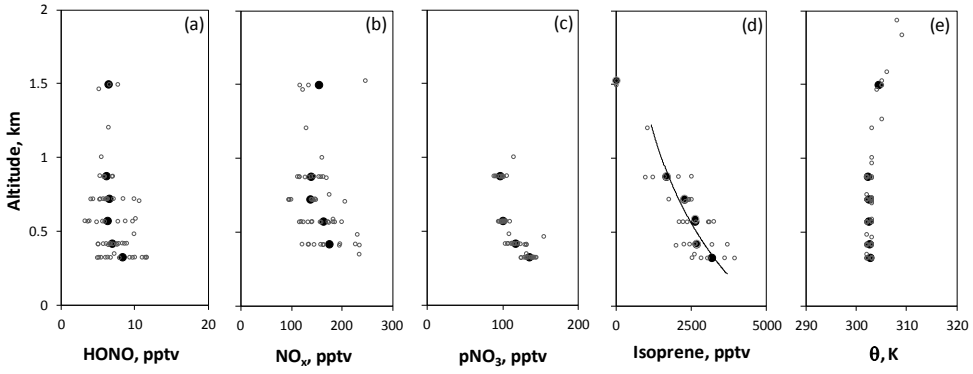

708

709 Figure 4. Vertical distributions of concentrations of HONO (a), NO_x (b), pNO_3 (c), isoprene
710 (d) and potential temperature (e) in the PBL during the first race-track of RF#4 from 11:00 –
711 12:15 LT (16:00 – 17:15 UTC), June 12, 2013. The small open circles represent the 1-min
712 data points, the large solid circles the mean values for each race-track measurement altitude.
713 The line in (d) is the best fit of (Eq. 1) to the isoprene data: $h = 5.97 - 0.692 \ln C$, $r^2 = 0.93$.

714

715

716

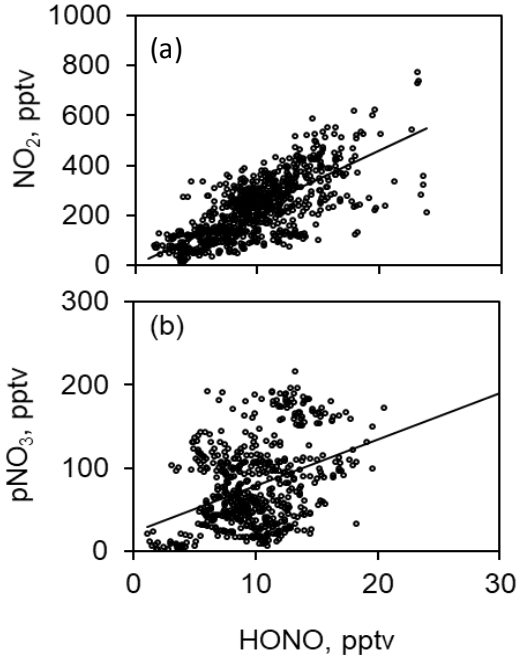

717

718

719 Figure 5. Correlation analysis of HONO with NO_x (a, r^2=0.52) and pNO_3 (b, r^2 = 0.14) in the
720 southeast US during the NOMADSS 2013 summer study. Data points in the urban and power
721 plant plumes have been excluded.

722

723

724

725

Atmos. Chem. Phys. Discuss., https://doi.org/10.5194/acp-2018-105
Manuscript under review for journal Atmos. Chem. Phys.
Discussion started: 13 February 2018

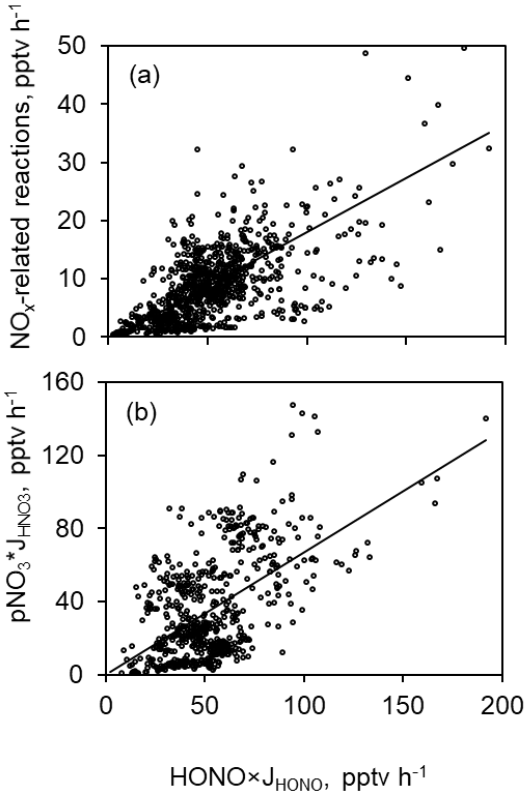

Figure 6. Correlation analysis of main HONO sink ("HONO×J_{HONO}") with contribution from particulate nitrate photolysis, $pNO_3 \times J_{pNO3}$ (a) and with contribution from NO_x related reactions (b) in the southeast US during the NOMADSS 2013 summer study. The line represents the least-squares fitting (R^2=0.44, intercept = -0.57 and slope = 0.19 for Figure 6a; R^2=0.31, intercept = 0.05 and slope = 0.67 for Figure 6b).

Atmos. Chem. Phys. Discuss., https://doi.org/10.5194/acp-2018-105
Manuscript under review for journal Atmos. Chem. Phys.
Discussion started: 13 February 2018

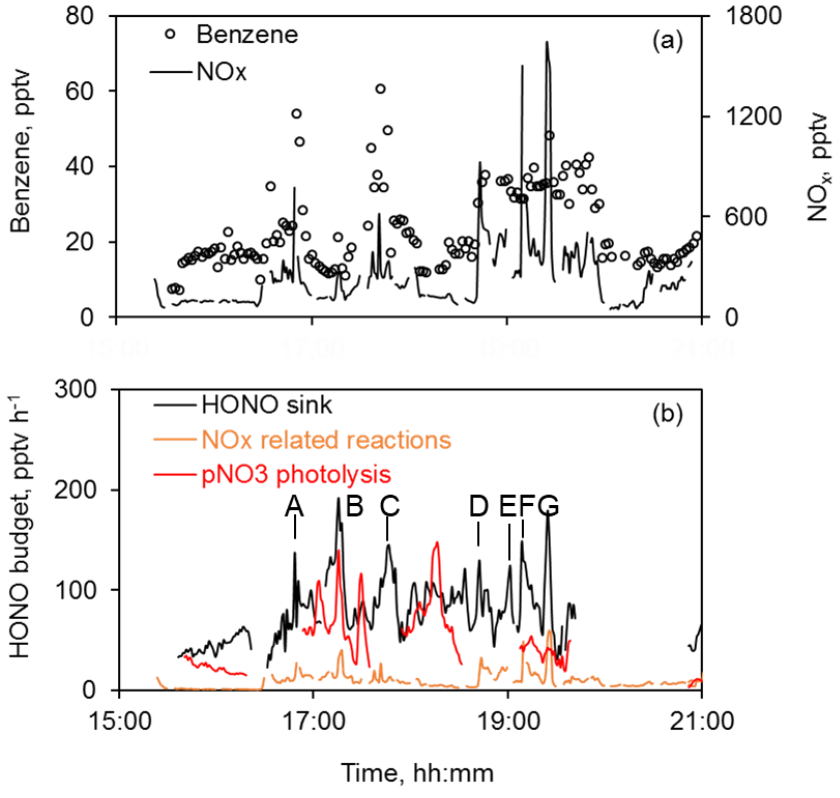

Figure 7. HONO budget analysis in RF #11 in the Southeast US during the NOMADSS 2013 summer study. "HONO sink" is the HONO loss rate contributed by photolysis and the reaction of HONO with OH radicals, "NOx related reactions" is the sum of HONO productions by all known NO_x reactions, and "pNO3 photolysis" is the HONO source contributed by photolysis of pNO_3

Atmos. Chem. Phys. Discuss., https://doi.org/10.5194/acp-2018-105
Manuscript under review for journal Atmos. Chem. Phys.
Discussion started: 13 February 2018

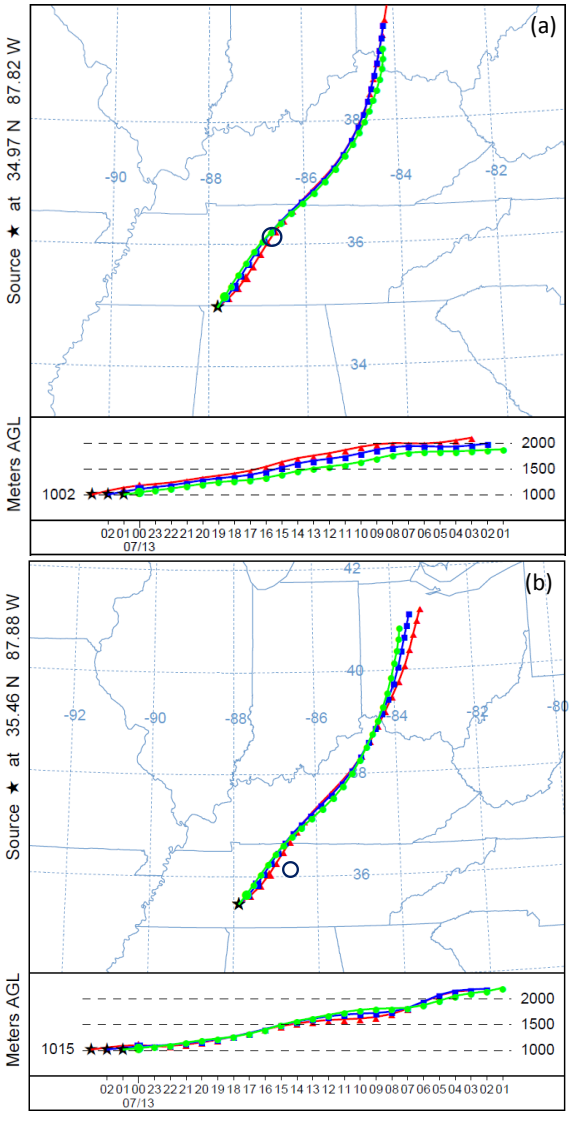

741

742 Figure 8. Back trajectory analysis of air masses encountered in the PBL in RF #18 in the
743 Southeast US during the NOMADSS 2013 summer study. The air masses arriving at the
744 southern point of the flight tracks were found to pass over the metropolitan area of Nashville
745 (the black circle, panel a), while those at the northern point to stay to the north of the area.
746 The back trajectory analysis was made using NOAA's online HYSPLIT model
747 (http://www.arl.noaa.gov/HYSPLIT_info.php).

748

Atmos. Chem. Phys. Discuss., https://doi.org/10.5194/acp-2018-105
Manuscript under review for journal Atmos. Chem. Phys.
Discussion started: 13 February 2018

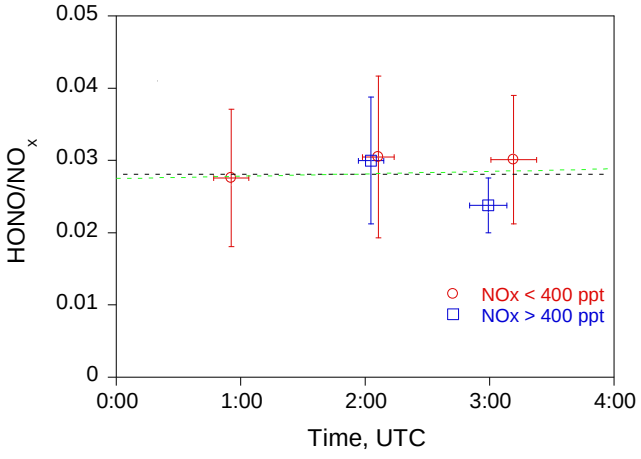

749

750 Figure 9. The evolution of HONO/NO_x ratio in the nocturnal boundary layer during the
751 RF#18. The red circles and blue squares are the median HONO/NO_x values under the
752 conditions of $NO_x \leq 400$ pptv and $NO_x > 400$ pptv, respectively. The horizontal bars indicate
753 the averaging time periods and the vertical bars the one standard deviation of HONO/NO_x
754 ratios. The black dashed line is the least squared fit to the data, and the green dashed line
755 indicates a slope of 3×10^{-4} hr^{-1}. The sunset time at the sampling location was 0:40 UTC.

756